Supporting Information

Physical properties of OLED host materials

Anirban Mondal [1,#], Leanne Paterson [1,#], Jaeyoung Cho [1,2], Kun-Han Lin [1], Bas van der Zee [1], Gert-Jan A. H. Wetzelaer [1], Andrei Stankevych [3], Alexander Vakhnin [3], Jang-Joo Kim [2], Andrey Kadashchuk [3,4], Paul W. M. Blom [1], Falk May, [5] and Denis Andrienko [1,*]

[1] Max Planck Institute for Polymer Research, Ackermannweg 10, 55128 Mainz, Germany

[2] Department of Materials Science and Engineering and the Center for Organic Light Emitting Diode, Seoul National University, Seoul, 151-744, South Korea

[3] Institute of Physics, Natl. Academy of Sciences of Ukraine, Prospect Nauky 46, 03028 Kyiv, Ukraine

[4] IMEC, Kapeldreef 75, B-3001 Leuven, Belgium

[5] Merck KGaA, 64293 Darmstadt, Germany

[#] these authors contributed equally to the work

[*] E-mail: denis.andrienko@mpip-mainz.mpg.de

System	λ_{holes}	$\lambda_{electrons}$
BCP	0.41	0.41
CBP	0.13	0.53
mCBP	0.05	0.53
mCP	0.08	0.11
MTDATA	0.45	0.19
NBPhen	0.17	0.27
NPB	0.31	0.17
Spiro-TAD	0.22	0.27
TCTA	0.24	0.15
TMBT	0.13	0.28
TPBi	0.25	0.39
2-TNATA	0.42	0.12

Table S1 Reorganisation energies (λ) for holes and electrons, listed for each of the systems, calculated by DFT using B3LYP/6-311+g(d,p) level of theory

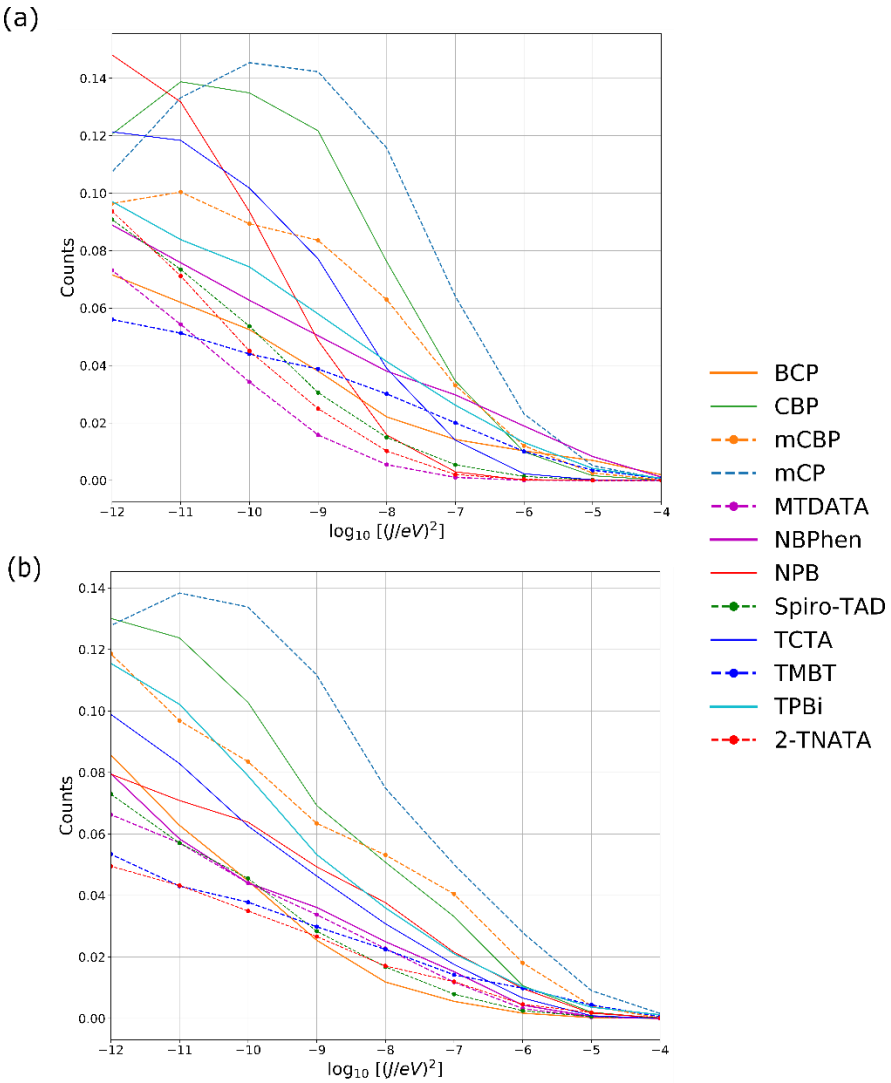

Figure S1 Distributions of the logarithm of the transfer integral *J* for (a) hole and (b) electron transport constructed from diabatic states based on the whole molecule.

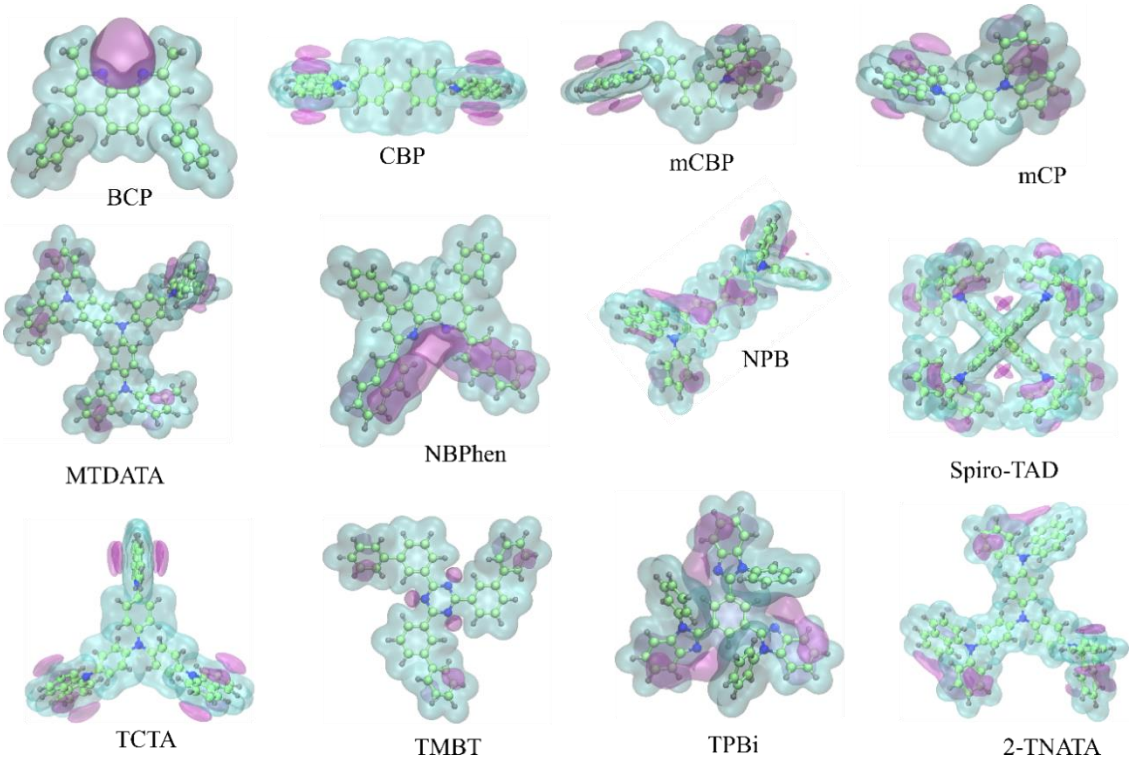

Figure S2 Iso-electrostatic potential surfaces, which are primarily responsible for the solid-state contribution to the ionization energy and the width of the density of states, for the organic semiconductors investigated in this work; BCP, CBP, mCBP, mCP, MTDATA, NBPhen, NPB, TCTA, TMBT, TPBi, Spiro-TAD and 2-TNATA.

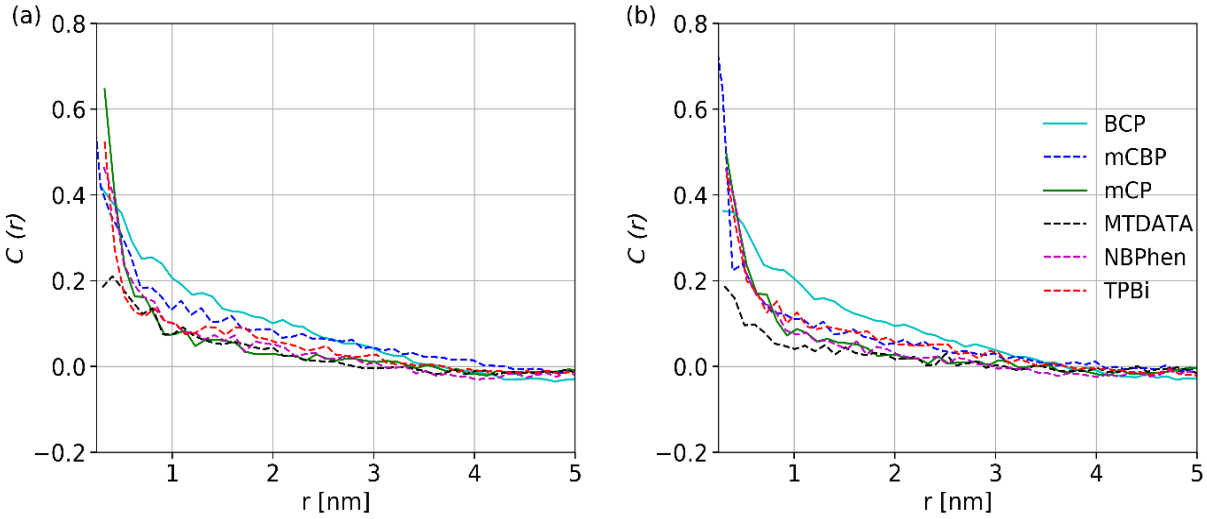

Figure S3 Site energy correlations for (a) holes and (b) electrons as a function of intermolecular distance in the amorphous organic semiconductors.

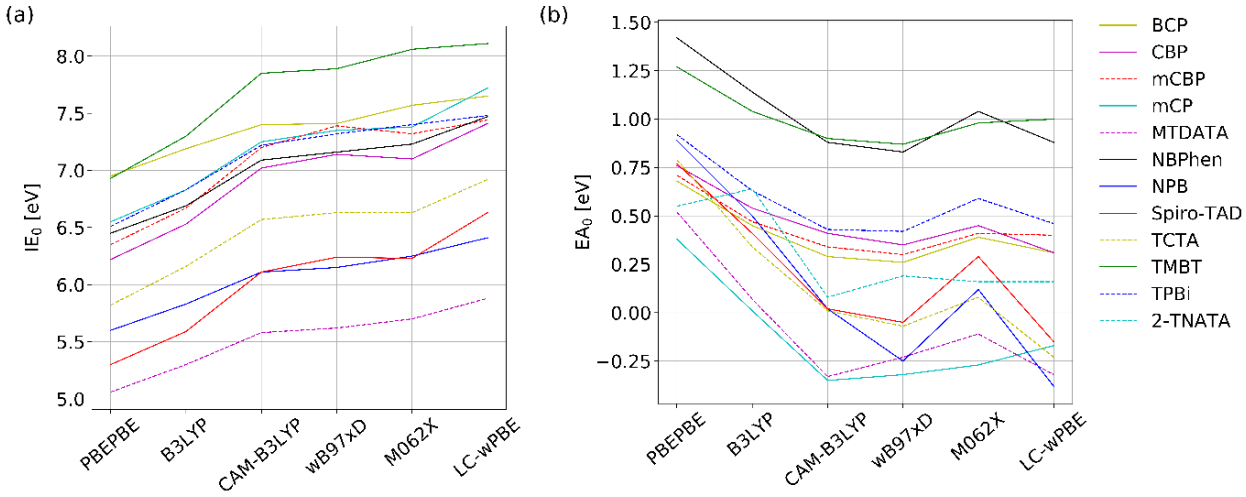

Figure S4 Gas phase (a) ionisation energies (IE_0) and electron affinities (EA_0) of the twelve organic semiconductors, as a function of DFT functionals, with the basis set 6-311+g(d,p).

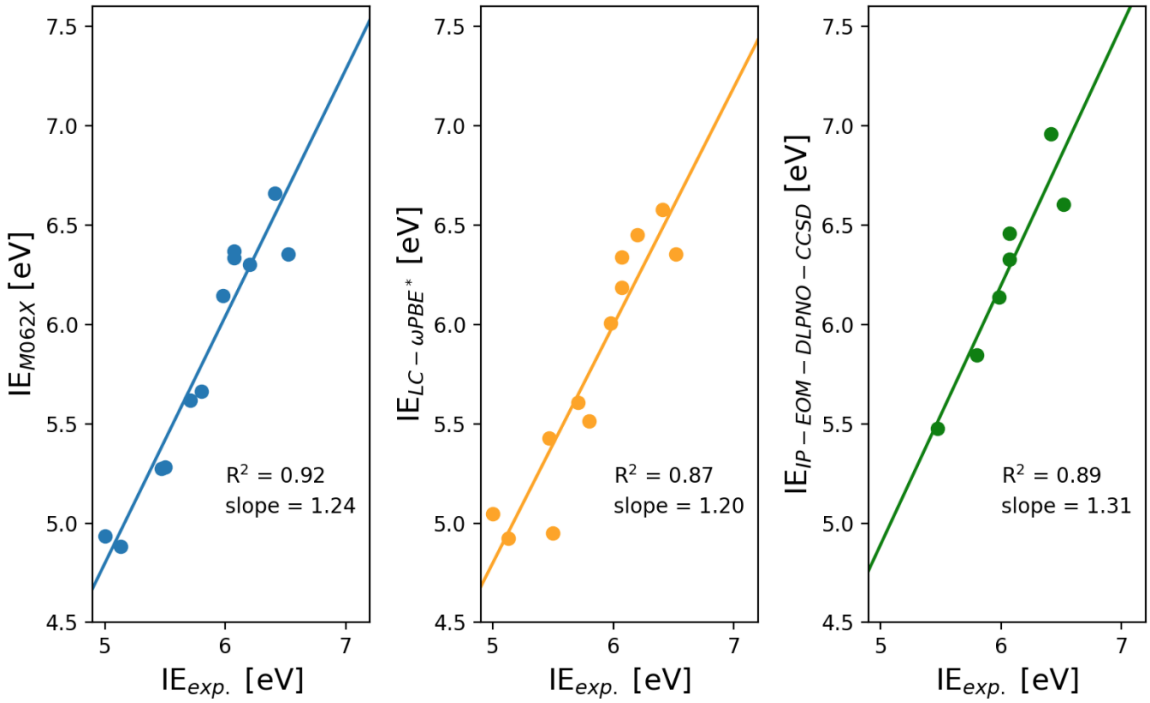

Figure S5 Comparison of experimental ionisation energies (IE_{exp}) and simulated (solid state) ionisation energies (IE_{tot}), with the gas phase (IE_0) obtained from different levels of theory: M062X/6-311+G(d,p), ω-tuned LC-ωPBE(LC-ωPBE*)/may-cc-pVTZ[1] and IP-EOM-DLPNO-CCSD/aug-cc-pVTZ.[2]

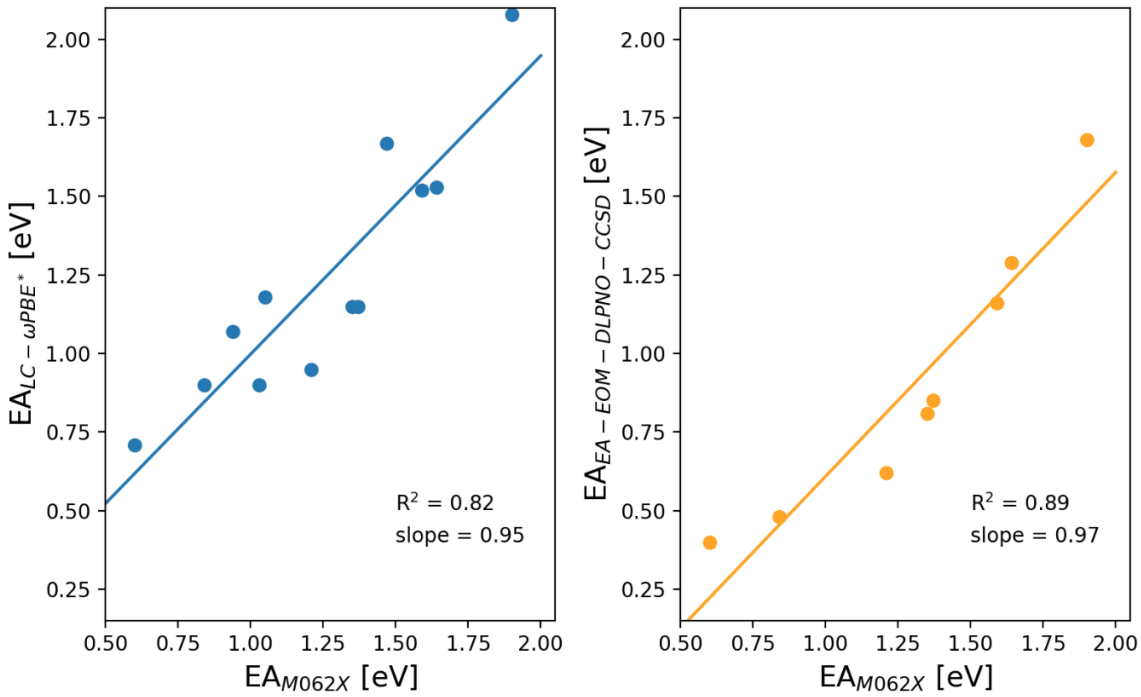

Figure S6 Simulated (solid state) electron affinity (EA_{tot}) with the gas phase (EA_0) obtained from different levels of theory: M06-2X/6-311+G(d,p), ω-tuned LC-ωPBE(LC-ωPBE*)/may-cc-pVTZ[1] and EA-EOM-DLPNO-CCSD/aug-cc-pVTZ.[3] Due to the lack of experimental data, the comparison is made between M062X and other levels of theory.

System	EA_0		IE_0		Optimal ω
	LC-ωPBE*	EA-EOM-DLPNO-CCSD	LC-ωPBE*	IP-EOM-DLPNO-CCSD	
BCP	0.26	NA	7.57	7.82	0.176
CBP	0.23	-0.07	7.07	7.19	0.177
mCBP	0.15	-0.18	7.17	7.31	0.180
mCP	-0.16	-0.47	7.24	7.37	0.180
MTDATA	0.02	NA	5.74	NA	0.141
NBPhen	0.97	0.61	7.08	7.41	0.150
NPB	0.18	-0.24	6.40	6.45	0.175
Spiro-TAD	0.42	NA	5.90	NA	0.125
TCTA	0.26	-0.14	6.62	NA	0.152
TMBT	0.87	0.63	7.98	8.36	0.173
TPBi	0.39	0.05	7.55	NA	0.157
2-TNATA	0.36	NA	5.83	NA	0.150

Table S2 IE_0 and EA_0 (eV) obtained at LC-ωPBE*/may-cc-pVTZ and IP/EA-EOM-DLPNO-CCSD/aug-cc-pVTZ. The optimal ω for each compound is also listed ($Bohr^{-1}$). Due to the limit of system size, we do not have values for all compounds using EOM-DLPNO-CCSD method (listed as NA).

IE_0/EA_0 Technical details:

To reduce the self-interaction error in DFT, it has been proposed to take ω in range-separated functionals as a parameter for further optimization. The optimization procedure for IE utilizes the fact that minus HOMO of a system equal to its IE in exact density functional theory. The ω that fulfils this criterion is then considered the optimal ω that significantly reduces the self-interaction error. This ω-tuned optimization procedure for IE has been extended to have a balance description for charge-transfer states[4] and HOMO-LUMO gap.[1] This is achieved by introducing the target function (*J*) to be minimized, defined as

$$J = |IE_N + \epsilon_{N,HOMO}| + |IE_A + \epsilon_{A,HOMO}|$$

where the capital N and A stands for the neutral and anionic states, respectively. Here we followed a protocol similar to that proposed by Brédas *et al*.[1] The anionic and neutral ground state geometries were optimized at the ωB97XD/6-311G(d,p) level. The ω-tuning procedure was performed using LC-ωPBE/may-cc-pVTZ. The optimal ω for each compound is shown in Table S2.

Another way to avoid the self-interaction error in DFT is to adopt a wavefunction-based method. The IP/EA-EOM-DLPNO-CCSD method has shown to be an affordable method for large molecules with a reasonable accuracy.[2,3] We hereby utilized these methods for IE_0/EA_0 computations. For details of the setting, we used aug-cc-pVTZ basis set with AutoAux (or def2/JK in case of convergence issue) and aug-cc-pVTZ/C auxiliary basis set. The Normal PNO scheme was used and the CutPNO Singles is set to 1e-10.

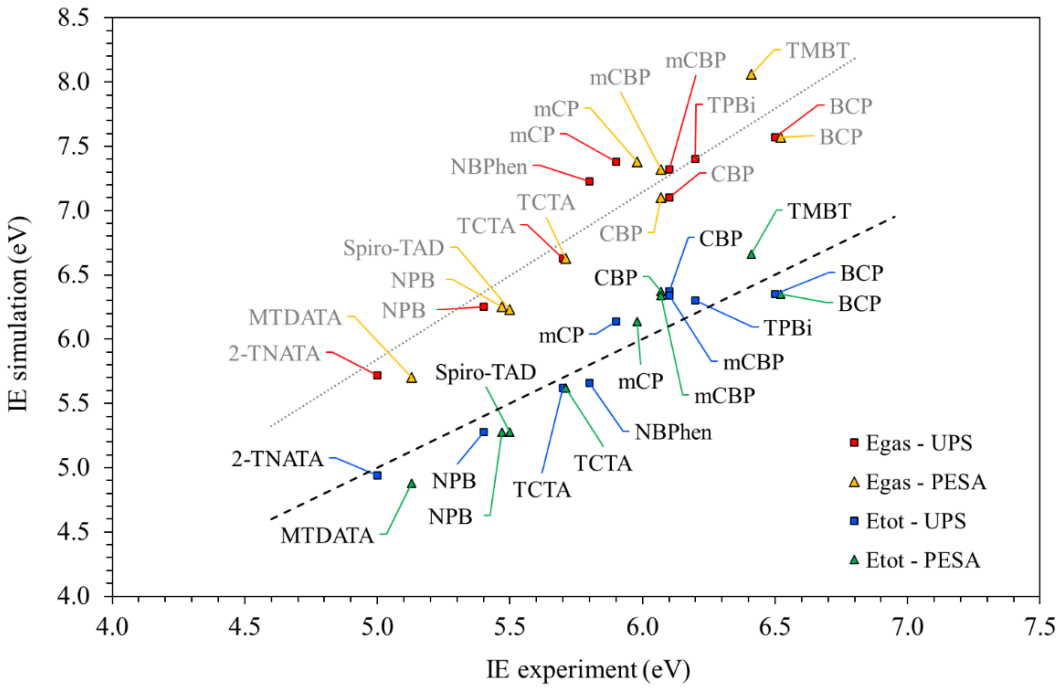

Figure S7 Simulated gas phase ionisation energies (Egas) compared with experimental UPS: red squares (R^2=0.878) & PESA: yellow triangles (R^2=0.925). Simulated solid-state ionisation energies (Etot) compared with experimental UPS: blue squares (R^2=0.899) & PESA: green triangles (R^2=0.911). The linear relationship (x=y) is shown by the black dashed line, highlighting the correlation of experimental and simulated solid state ionisation energies. For comparison, the grey dashed line is used as a visual aid to show the shift of gas phase ionisation energies.

Cyclic Voltammetry (CV) measurements:

For Cyclic Voltammetry measurements at Merck KGaA, Darmstadt, Germany we have used a potentiostat from Metronom µAUTOLAB type III in a three-electrode setup including working-electrode (Au), counter electrode (Pt) and reference-electrode (Ag/AgCl, KCl 3 M). Oxidation was measured in DCM and reduction in THF and tetrabutylammonium hexafluorophosphate (0.11 M) was added as electrolyte. As internal standard we have used ferrocene or decamethylferrocene. Ionisation energies (IE) and electron affinities (EA) were calculated according to the following relationships where Eox and ERed are taken as half-step potential.[5]

$$IE = -4.8\ eV - Eox\ vs.\ Fc/Fc+$$

$$EA = -4.8\ eV - ERed\ vs.\ Fc/Fc+$$

Errors for single IE measurements are +-0.01eV as we have analysed for repeated measurements for independently prepared solutions of the same material. In case of EA, the lower conductivity of THF as compared to DCM leads to stronger voltage drop in the solution

which broadens the reduction peaks and leads to a larger error of +-0.02eV for EA measurements. These errors are estimated for reversible and well resolvable oxidation/reduction peaks and will increase in case of multiple (overlapping) peaks or if EA or IP are close to the limit of measurable potential range.

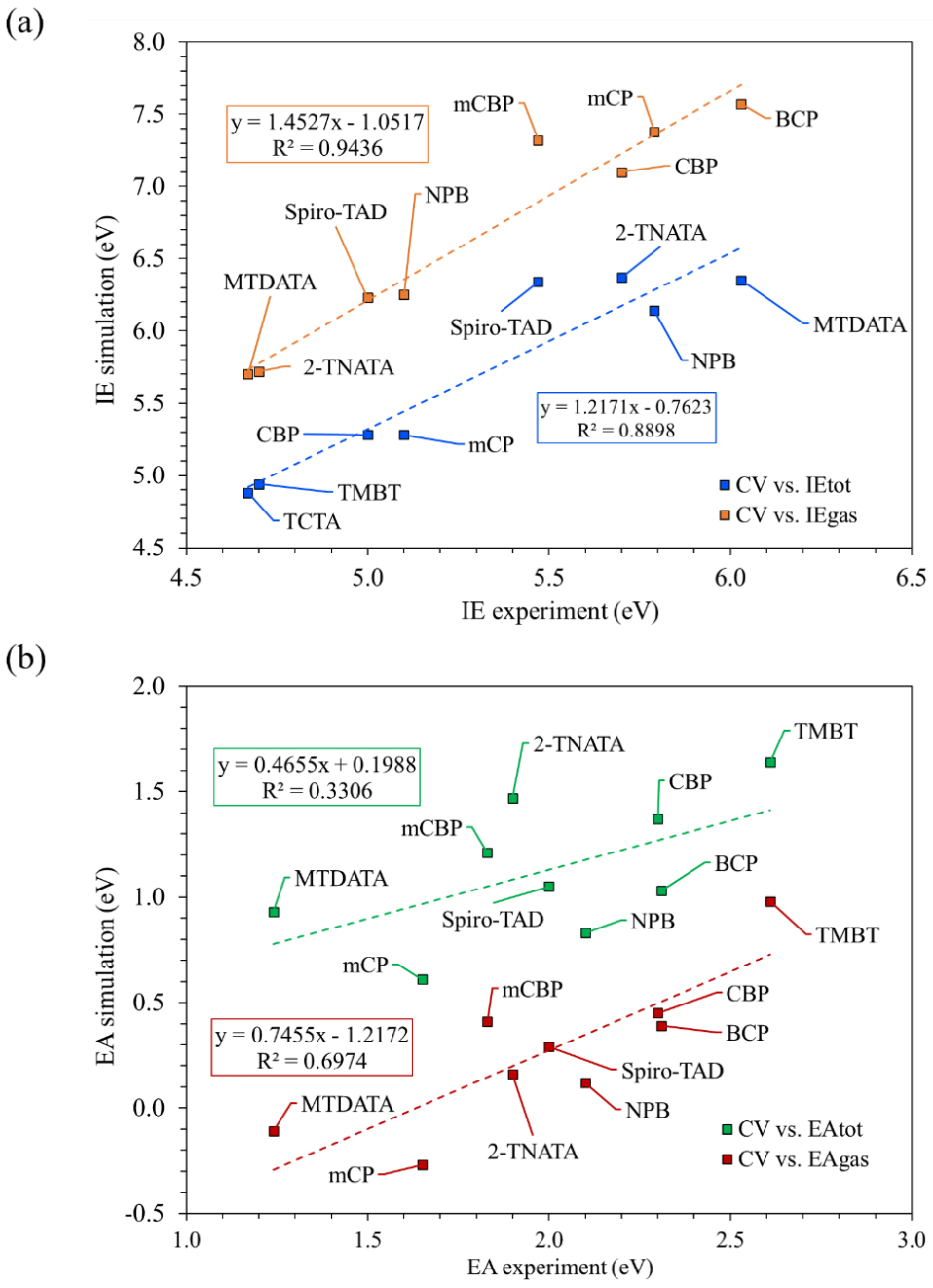

Figure S8 (a) Experimental CV (HOMO) data compared with simulated gas phase ionisation energy (IE_{gas}) orange (R^2=0.9436) and simulated solid state ionisation energy (IE_{tot}) blue (R^2=0.8898). (b) Experimental CV (LUMO) data compared with simulated gas phase electron affinity (EA_{gas}) red (R^2=0.6974) and simulated solid state electron affinity (EA_{tot}) green (R^2=0.3306). The dashed lines are the lines of best fit for the values of matching colour, to serve as a visual aid.

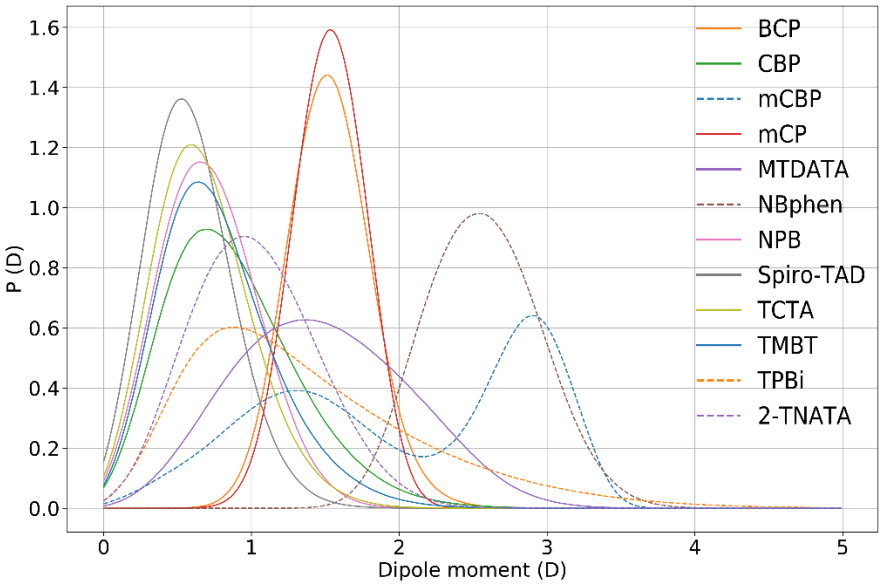

Figure S9 Distribution of molecular dipoles in the amorphous morphology for the twelve organic materials, calculated from MD simulations at 300K, with the partial charges obtained by GDMA.

System	d DFT	<d> MD	std(d) MD
BCP	2.91	1.53	0.24
CBP	0.0001	0.87	0.43
mCBP	0.95	2.03	0.87
mCP	1.27	1.52	0.20
MTDATA	0.79	1.48	0.57
NBPhen	3.43	2.56	0.36
NPB	0.31	0.71	0.30
Spiro-TAD	0.001	0.58	0.26
TCTA	0.01	0.67	0.31
TMBT	0.01	0.77	0.37
TPBi	6.33	1.89	1.86
2-TNATA	0.56	1.02	0.40

Table S3 Dipole moment (d) (Debye) of an isolated molecule obtained from quantum chemical calculations (DFT) using M062X/6-311+g(d,p) level of theory (d DFT). The average dipole moment from molecular dynamics simulations, calculated at 300K, using the partial charges obtained by GDMA[6] (<d> MD) with standard deviation (std(d) MD).

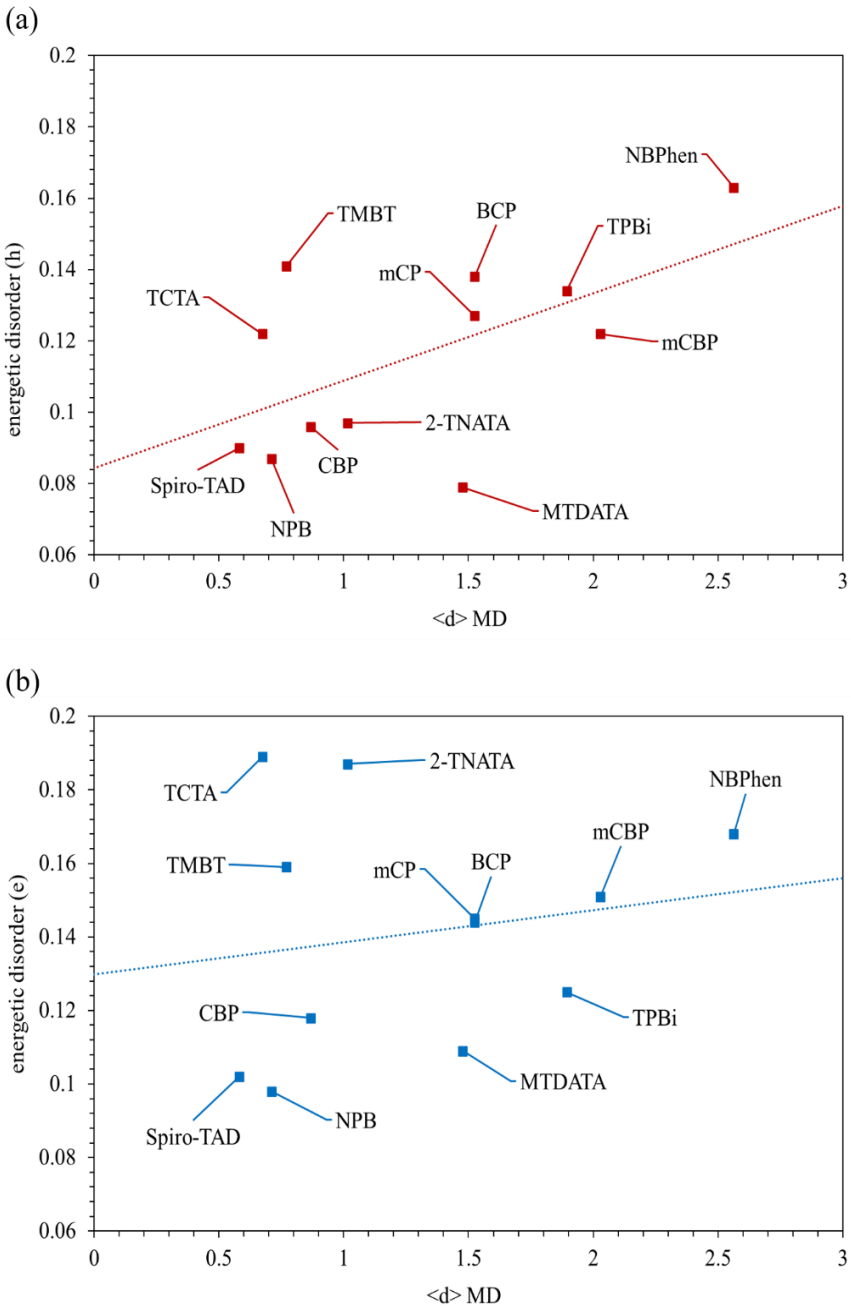

Figure S10 The average dipole moment from molecular dynamics simulations, calculated at 300K, using the partial charges obtained by GDMA ($\langle d \rangle$, MD), plotted against the energetic disorder for the twelve systems, for (a) holes and (b) electrons. The dashed lines are lines of best fit, to serve as a visual aid of the correlation.

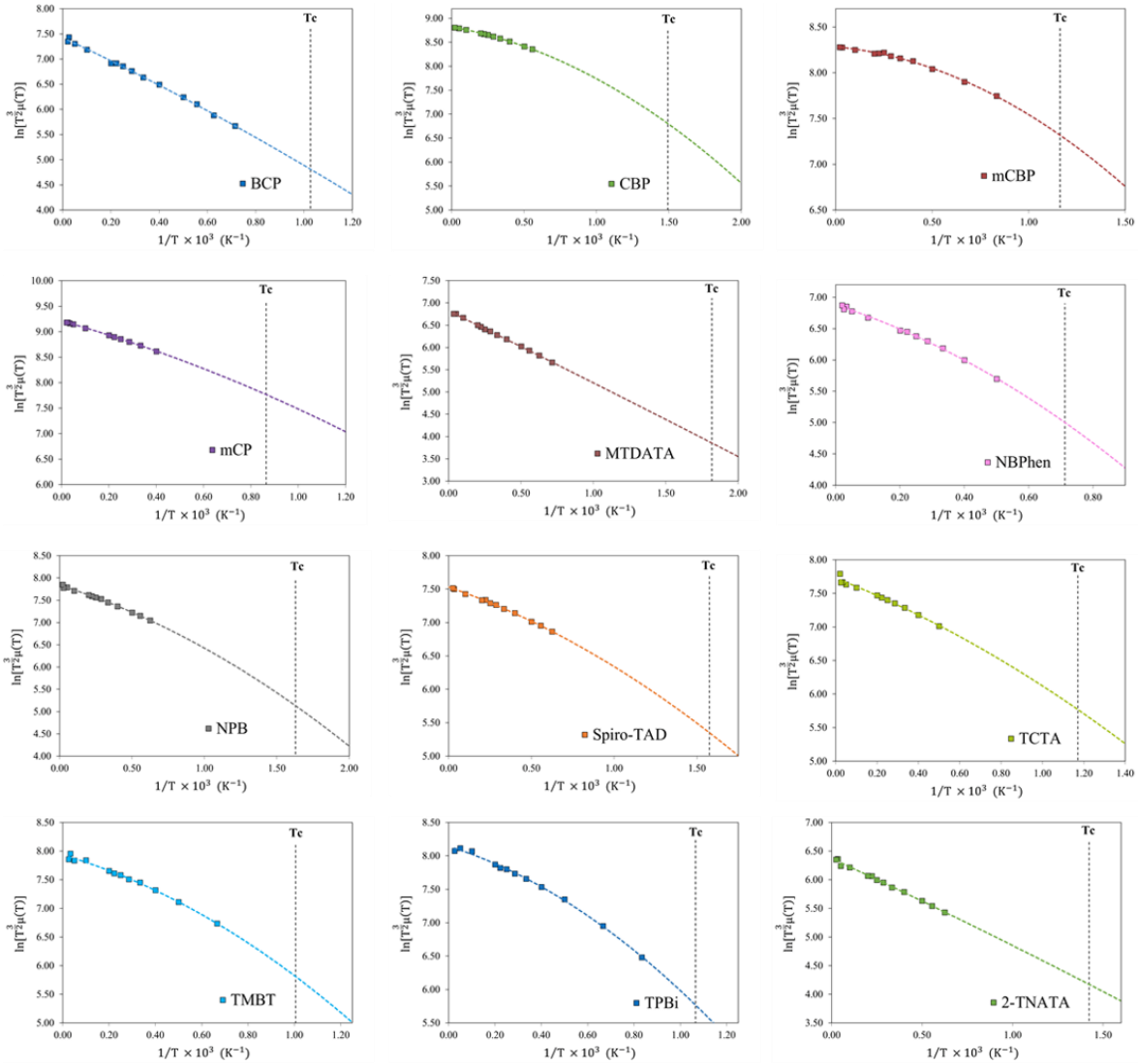

Figure S11 Hole mobility temperature dependence for the twelve systems, including the estimated critical temperature (within Gaussian Disorder model) Tc, at which the transition from dispersive to nondispersive regime takes place (dashed black line). Calculated for one charge carrier (hole) at a range of high temperatures, with an applied field F = $1x10^4$ V/cm. Further information regarding the temperature dependence, explanation of the fitting procedure and extraction of room temperature mobilities, can be found here.[7]

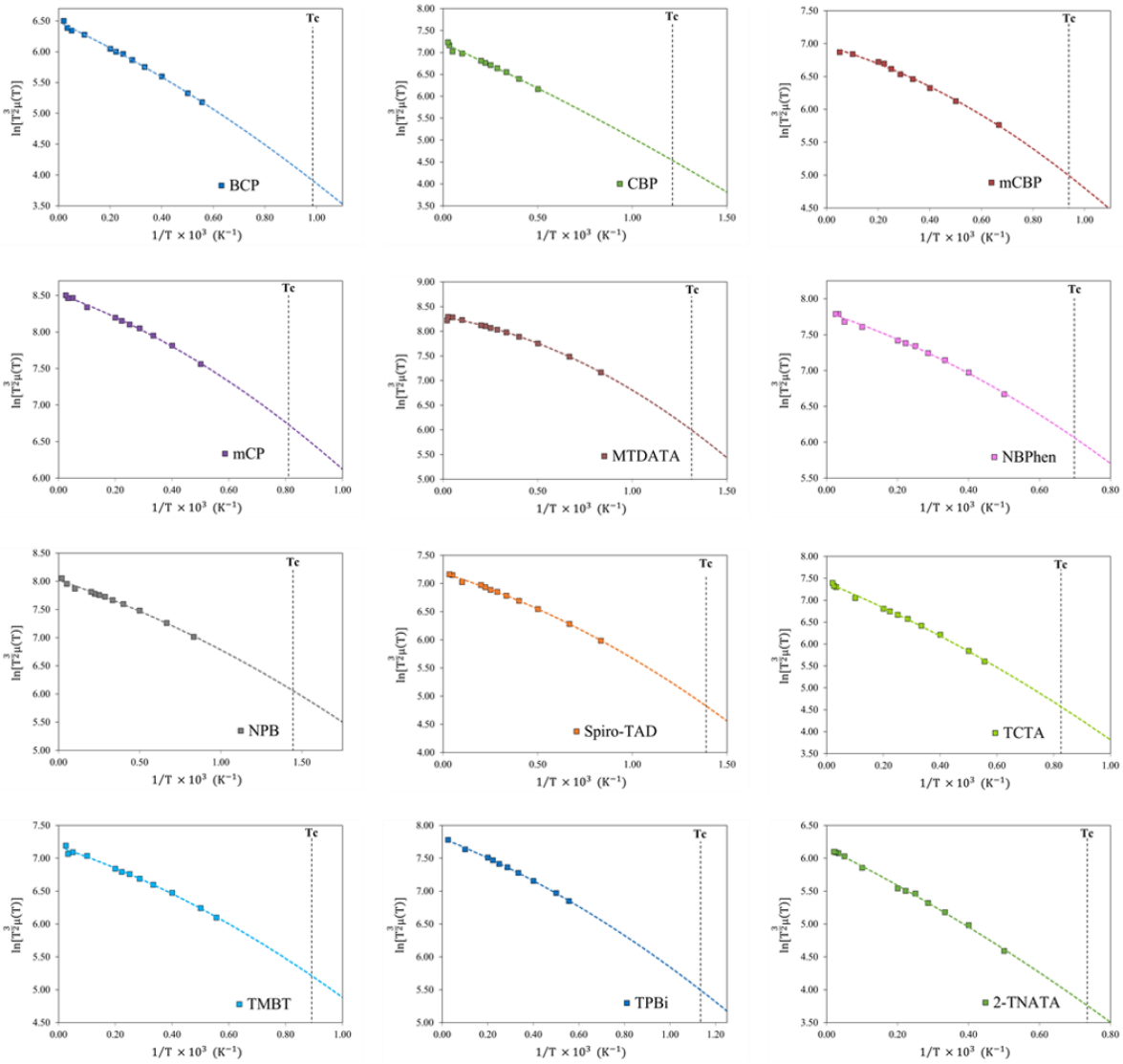

Figure S12 Electron mobility temperature dependence for the twelve systems, including the estimated critical temperature (within Gaussian Disorder model) Tc, at which the transition from dispersive to nondispersive regime takes place (dashed black line). Calculated for one charge carrier (electron) at a range of high temperatures, with an applied field F = $1x10^4$ V/cm. Further information regarding the temperature dependence, explanation of the fitting procedure and extraction of room temperature mobilities, can be found here.[7]

Glass Transition temperature – linear fitting procedure:

To reduce human error and any inaccuracies in choosing the range for linear fitting, we plotted the R^2 value as a function of temperature with a 200 K range (see Figure S13), i.e. [T-200, T] for $T \in [200, 800]$. The valley observed in such a plot characterises the non-linear transition in the density-temperature plot. We define the hill tops (maximum R^2 value) on two opposite sides of the valley as the optimal fitting ranges.

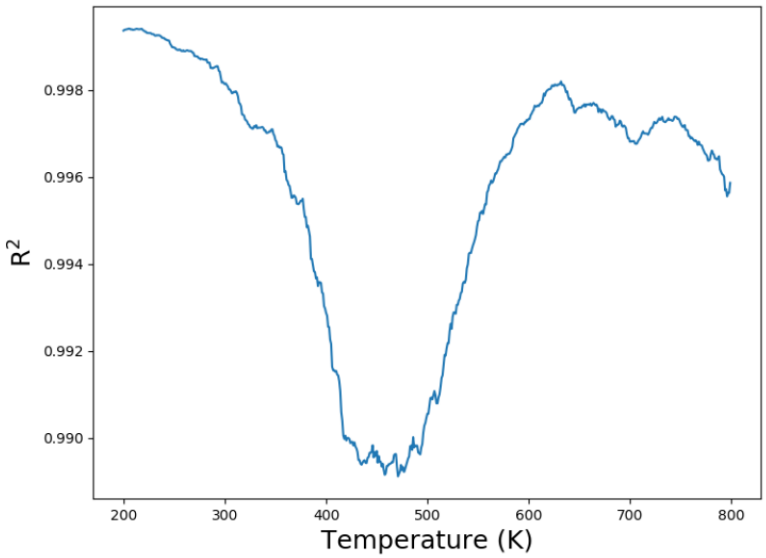

Figure S13 R^2 as a function of temperature with a range of 200K [T-200, T].

Thermally stimulated luminescence (TSL)

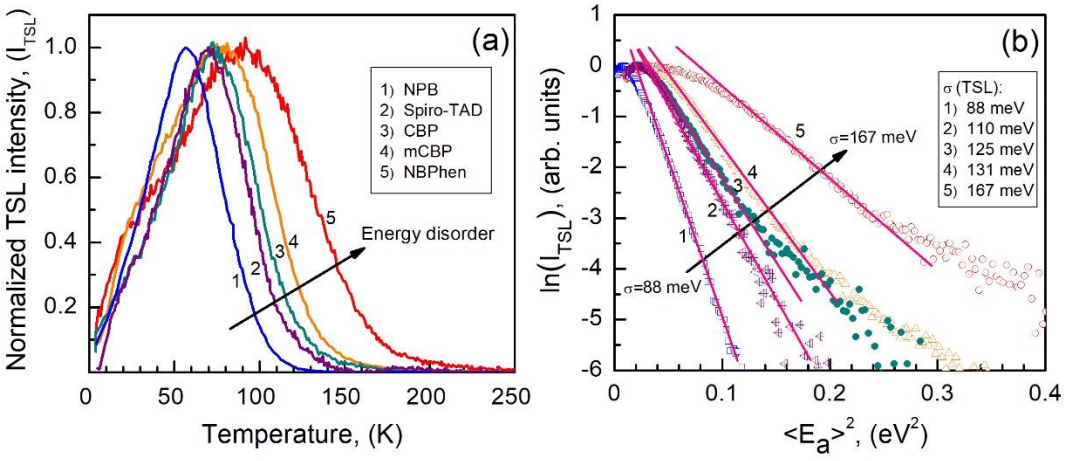

Figure S14(a) Normalized spectrally integrated TSL glow curve measured at the constant heating rate 0.15 K/s after excitation with 313nm-light for 3 min at 4.2 K in NPB, Spiro-TAD, CBP, mCBP, and NBPhen films (curve 1, 2, 3, 4, 5, respectively). (b) "Gaussian" analysis of high temperature wings of the TSL curves shown in (a). The temperature scale was converted to a trap energy scale <Ea>(T) using the following empirical calibration relation <Ea>=0.0032×T-0.091 (in eV) (see [8] for details) obtained by fractional TSL measurements, and then the high-temperature part of the TSL signal intensity was plotted logarithmically against <Ea>2. The slope of the straight lines is a measure of the DOS width, and the extracted σ-parameters for the above materials are listed in the Inset. More details about the TSL data analysis can be found elsewhere.[9]

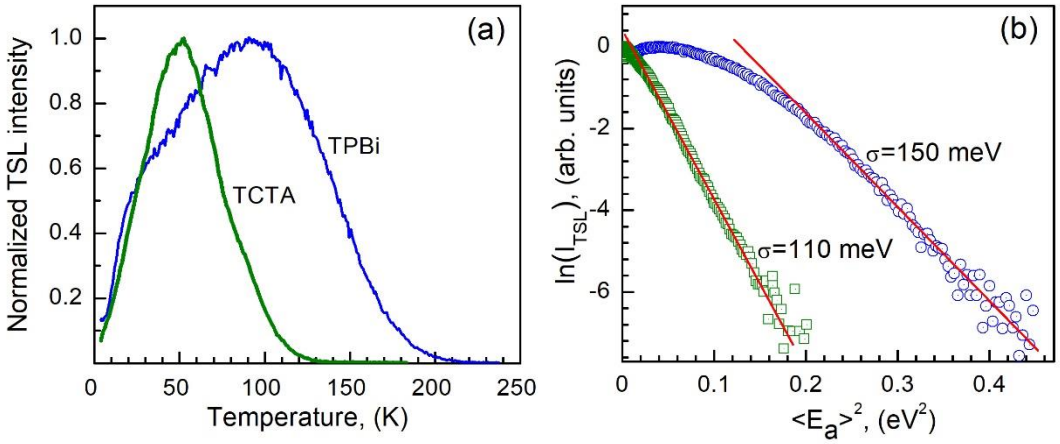

Figure S15 (a) Normalized spectrally integrated TSL glow curve measured at the constant heating rate 0.15 K/s after excitation with 313nm-light for 3 min at 4.2 K in TCTA and TPBi films (curve 1 and 2, respectively). (b) "Gaussian" analysis of high temperature wings of the TSL curves shown in (a), which is done using the same procedure as mentioned in Figure S14(b).

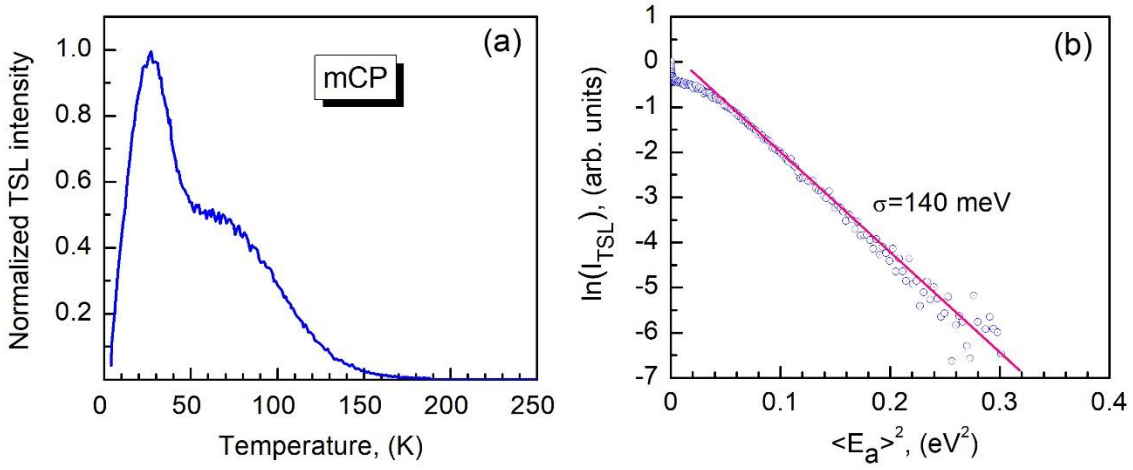

Figure S16 (a) Normalized spectrally integrated TSL glow curve measured after excitation with 313nm-light for 3 min at 4.2 K in a mCP film. (b) "Gaussian" analysis of high temperature wings of the TSL curve shown in (a), which is done using the same procedure as mentioned in Figure S14(b).

References

(1) Sun, H.; Ryno, S.; Zhong, C.; Ravva, M. K.; Sun, Z.; Körzdörfer, T.; Brédas, J.-L. Ionization Energies, Electron Affinities, and Polarization Energies of Organic Molecular Crystals: Quantitative Estimations from a Polarizable Continuum Model (PCM)-Tuned Range-Separated Density Functional Approach. *J. Chem. Theory Comput.* **2016**, *12* (6), 2906–2916. https://doi.org/10.1021/acs.jctc.6b00225.

(2) Dutta, A. K.; Saitow, M.; Riplinger, C.; Neese, F.; Izsák, R. A Near-Linear Scaling Equation of Motion Coupled Cluster Method for Ionized States. *The Journal of Chemical Physics* **2018**, *148* (24), 244101. https://doi.org/10.1063/1.5029470.

(3) Dutta, A. K.; Saitow, M.; Demoulin, B.; Neese, F.; Izsák, R. A Domain-Based Local Pair Natural Orbital Implementation of the Equation of Motion Coupled Cluster Method for Electron Attached States. *J. Chem. Phys.* **2019**, *150* (16), 164123. https://doi.org/10.1063/1.5089637.

(4) Stein, T.; Kronik, L.; Baer, R. Reliable Prediction of Charge Transfer Excitations in Molecular Complexes Using Time-Dependent Density Functional Theory. *J. Am. Chem. Soc.* **2009**, *131* (8), 2818–2820. https://doi.org/10.1021/ja8087482.

(5) Dandrade, B.; Datta, S.; Forrest, S.; Djurovich, P.; Polikarpov, E.; Thompson, M. Relationship between the Ionization and Oxidation Potentials of Molecular Organic Semiconductors. *Organic Electronics* **2005**, *6* (1), 11–20. https://doi.org/10.1016/j.orgel.2005.01.002.

(6) Stone, A. J. Distributed Multipole Analysis: Stability for Large Basis Sets. *J. Chem. Theory Comput.* **2005**, *1* (6), 1128–1132. https://doi.org/10.1021/ct050190+.

(7) Lukyanov, A.; Andrienko, D. Extracting Nondispersive Charge Carrier Mobilities of Organic Semiconductors from Simulations of Small Systems. *Phys. Rev. B* **2010**, *82* (19), 193202. https://doi.org/10.1103/PhysRevB.82.193202.

(8) Stankevych, A.; Andrienko, D.; Paterson, L.; Genoe, J.; Fishchuk, I. I.; Bässler, H.; Köhler, A.; Kadashchuk, A. Density of States of OLED Hosts from Thermally Stimulated Luminescence. *Phys. Rev. Appl.* **2020**.

(9) Kadashchuk, A.; Weiss, D. S.; Borsenberger, P. M.; Nešpùrek, S.; Ostapenko, N.; Zaika, V. The Origin of Thermally Stimulated Luminescence in Neat and Molecularly Doped Charge Transport Polymer Systems. *Chemical Physics* **1999**, *247* (2), 307–319. https://doi.org/10.1016/S0301-0104(99)00169-X.